Bimetallic Microswimmers Speed Up in Confining Channels

Chang Liu,[1] Chao Zhou,[2] Wei Wang,[2,3] and H. P. Zhang[1,4,*]

[1]Department of Physics and Astronomy and Institute of Natural Sciences, Shanghai Jiao Tong University, Shanghai 200240, China
[2]School of Material Science and Engineering, Harbin Institute of Technology, Shenzhen Graduate School, Shenzhen 518055, China
[3]Center for Soft and Living Matter, Institute for Basic Science (IBS), Ulsan 44919, Republic of Korea
[4]Collaborative Innovation Center of Advanced Microstructures, Nanjing 210093, China

(Received 15 June 2016; revised manuscript received 22 September 2016; published 3 November 2016)

Synthetic microswimmers are envisioned to be useful in numerous applications, many of which occur in tightly confined spaces. It is therefore important to understand how confinement influences swimmer dynamics. Here we study the motility of bimetallic microswimmers in linear and curved channels. Our experiments show swimmer velocities increase, up to 5 times, with the degree of confinement, and the relative velocity increase depends weakly on the fuel concentration and ionic strength in solution. Experimental results are reproduced in a numerical model which attributes the swimmer velocity increase to electrostatic and electrohydrodynamic boundary effects. Our work not only helps to elucidate the confinement effect of phoretic swimmers, but also suggests that spatial confinement may be used as an effective control method for them.

DOI: 10.1103/PhysRevLett.117.198001

Material transport at micro- or nanometer scales is conventionally driven by externally imposed fields, such as pressure or temperature [1,2]. In contrast, microorganisms move autonomously without external driving; they self-propel by converting local sources of energy into mechanical work [3–8]. Many synthetic microswimmers can mimic their biological counterparts in achieving autonomous motion [3–10]. For example, Janus particles generate local gradients of temperature [11], chemical concentration [12–14], or electric potential [15–19] and self-propel through respective phoretic mechanisms [20–22]. These phoretic microswimmers have demonstrated preliminary applications, such as cargo delivery [23,24], chemical sensing [25,26], and water purification [27,28]; they have also been recently used to explore the nonequilibrium physics of active matter [13,14,29].

Microswimmers are often required to move through narrow channel-like passages [30]. Hydrodynamic swimmers in such strong confinement have been investigated. Experiments showed that *Paramecium* [31] and *E. coli* bacteria [32] slow down in narrow channels; these results were later reproduced numerically [33,34]. Wu *et al.* showed numerically that amoeboid slows down in strong confinement [35]. Other numerical studies predicted that swimmer velocity may increase with confinement for a squirmer driven by normal deformations [33], a Taylor-like swimmer [36], and a rotating helix [37]. Ledesma *et al.* [38] reported that elasticity of confining boundary may speed up a dipolar swimmer. These studies show hydrodynamic interaction with confinement can lead to rich swimmer dynamics.

In contrast with the numerous studies of hydrodynamic swimmers [31–38], the subject of synthetic swimmers in confinement has remained largely unexplored until quite recently. Synthetic swimmers are found to strongly interact with boundaries, such as a flat plane [39–44], a corner [42,43,45], a colloid crystal [46], or a spherical confinement [47]. We are therefore motivated to investigate how strongly confining channels affect synthetic swimmers, particularly their motility. Our experiments show bimetallic swimmers significantly increase their velocity in channels. A numerical model reproduces our experimental results and reveals that the channels influence swimmers through electrostatic and electrohydrodynamic boundary effects. This knowledge not only helps us better understand the complex interplay between phoretic microswimmers and their environment, but also suggests control strategies for their practical applications in confined situations.

We fabricate two kinds of bimetallic microswimmers. One contains Au and Ru segments of equal length, the other Au and Rh segments. Both swimmers are rodlike and have a diameter $d_s = 0.3$ μm and different length, denoted as l_s (1.8 to 3.7 μm). A two-photon direct laser writing system fabricates microchannels with a submicron accuracy; the system's efficiency and flexibility allow us to systematically vary channel size and topology. Scanning electron images and detailed fabrication procedures can be found in the Supplemental Material [48]. After fabrication, we immerse swimmers and channels in a solution containing hydrogen peroxide (H_2O_2, 5% to 30% by weight). Swimmer motion in the sample is recorded through a 60× objective at a rate of 30 frames per sec with a camera (Basler acA2040-90um) and analyzed with standard particle tracking algorithms.

A bimetallic microswimmer propels through a self-electrophoretic mechanism. As sketched in Fig. 1(a)

(adapted from Ref. [18]), the oxidation and reduction of H_2O_2 occur preferentially at the anode and cathode, respectively. This results in an asymmetric distribution of electric potential and creates a field around the swimmer. The electric field then drives electro-osmotic flow on the negatively charged swimmer and propels the swimmer with the anode leading [15–19]. As shown in Fig. 1(c), an AuRu swimmer moves at a velocity around 19.8 μm/s outside channels in the open space or along a wall (the exterior boundary of the channel) [42,43,45], and it doubles its velocity after entering a linear and narrow channel with dimensions of $w = 1.2$ and $h = 2$ μm [cf. Fig. 1(b)]. We also test channels with different topologies; velocity increase is robustly observed in a spiral channel with a varying width and a square channel with segments of different width (cf. Supplemental Material [48]).

We quantify this speed-up phenomenon by normalizing the steady swimmer velocity in channels V by the velocity outside, $V_\circ$. The normalized velocity $V/V_\circ$ in linear channels is plotted versus the channel width for three sets of channels of different heights in Fig. 1(d). Results from spiral channels are similarly analyzed and shown in the Supplemental Material [48]. In both linear and spiral channels, a decrease in channel height or width leads to a higher swimmer velocity. Plotting the normalized velocity versus the channel cross-section area ($h \times w$), we can collapse data from channels of different heights into a single curve, as shown in the inset of Fig. 1(d).

Bimetallic microswimmer motility can be tuned by changing the concentration of H_2O_2 or by adding sodium nitrate ($NaNO_3$) to the solution; we take advantage of this tunablity to further investigate the effect of driving strength on confined swimmer motility. Concentrations of the two chemicals modulate swimmer velocity by different mechanisms: the former (H_2O_2) determines the reaction rate on the swimmer surface [53]; the latter ($NaNO_3$) mainly affects the system's electrostatic properties, such as double layer thickness and conductivity [54–57]. As shown in the insets of Figs. 1(e) and 1(f), with either of the two methods, we can change $V_\circ$ approximately by a factor of 2. However, such changes in $V_\circ$ do not lead to noticeable variations of the normalized swimmer velocity $V/V_\circ$, as shown in Figs. 1(e)–1(f). To briefly summarize, experimental results in Fig. 1 show that the swimmer velocity increase crucially

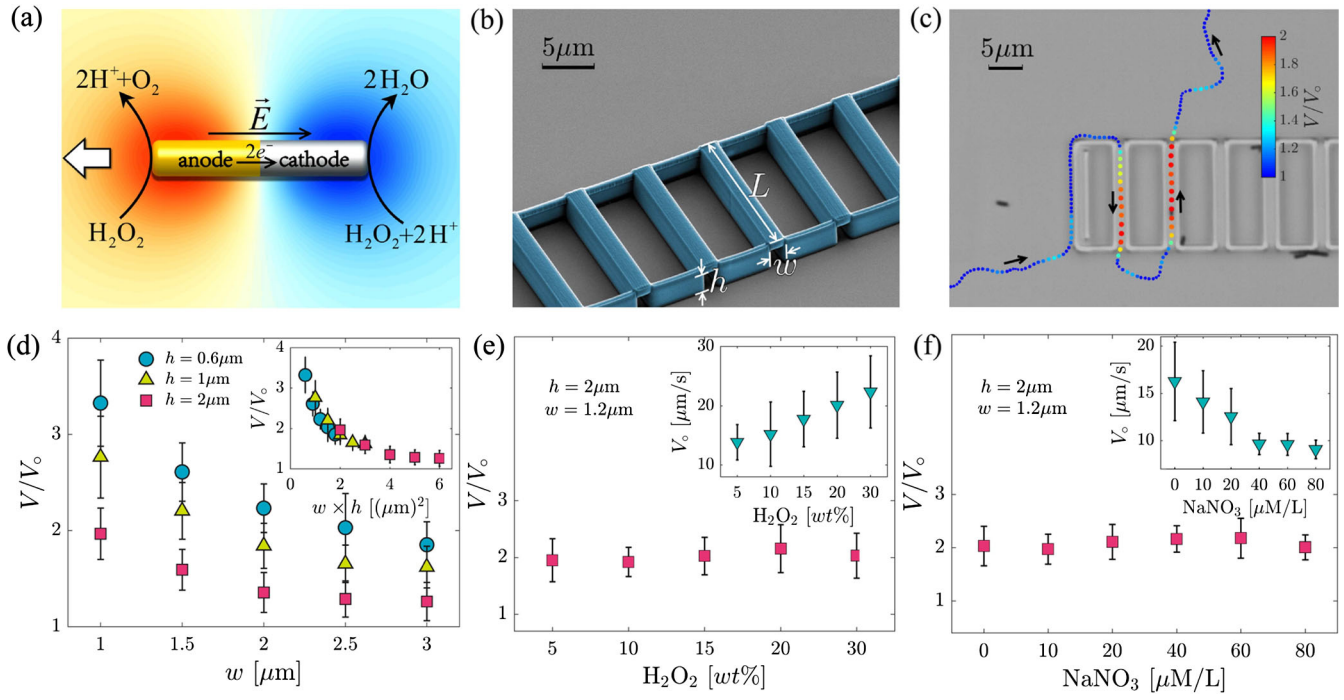

FIG. 1. Swimmer dynamics in linear channels. (a) Illustration of the self-electrophoretic propulsion mechanism. Orange and blue represent high and low electric potentials, respectively. The electric field $\vec{E}$ points from the anode end to the cathode, where the anode corresponds to the Au end in AuRu swimmers and the Rh end in AuRh swimmers. The white arrow indicates the direction of motion of the swimmer. (b) Scanning electron image of linear channels with a length L, width w, and height h. In (c), a typical AuRu swimmer trajectory is plotted on an optical image of channels; each dot represents an instantaneous position (separated by 1/30 sec in time) of the swimmer and is color coded by the normalized swimmer velocity $V/V_\circ$ (see text). In (d), the normalized swimmer velocity $V/V_\circ$ is plotted versus the channel width in the main frame and versus the channel cross-section area in the inset. (e) and (f) Normalized swimmer velocity versus the concentrations of H_2O_2 and $NaNO_3$. Swimmer velocity outside channels, $V_\circ$, is plotted in the insets. All linear channels have the same length of $L = 16$ μm. Solutions with 15% H_2O_2 are used to produce data in (c),(d), and (f). $NaNO_3$ is only used in experiments in (f). See supporting videos S1 to S4 in the Supplemental Material [48] for swimmer motion in different channels.

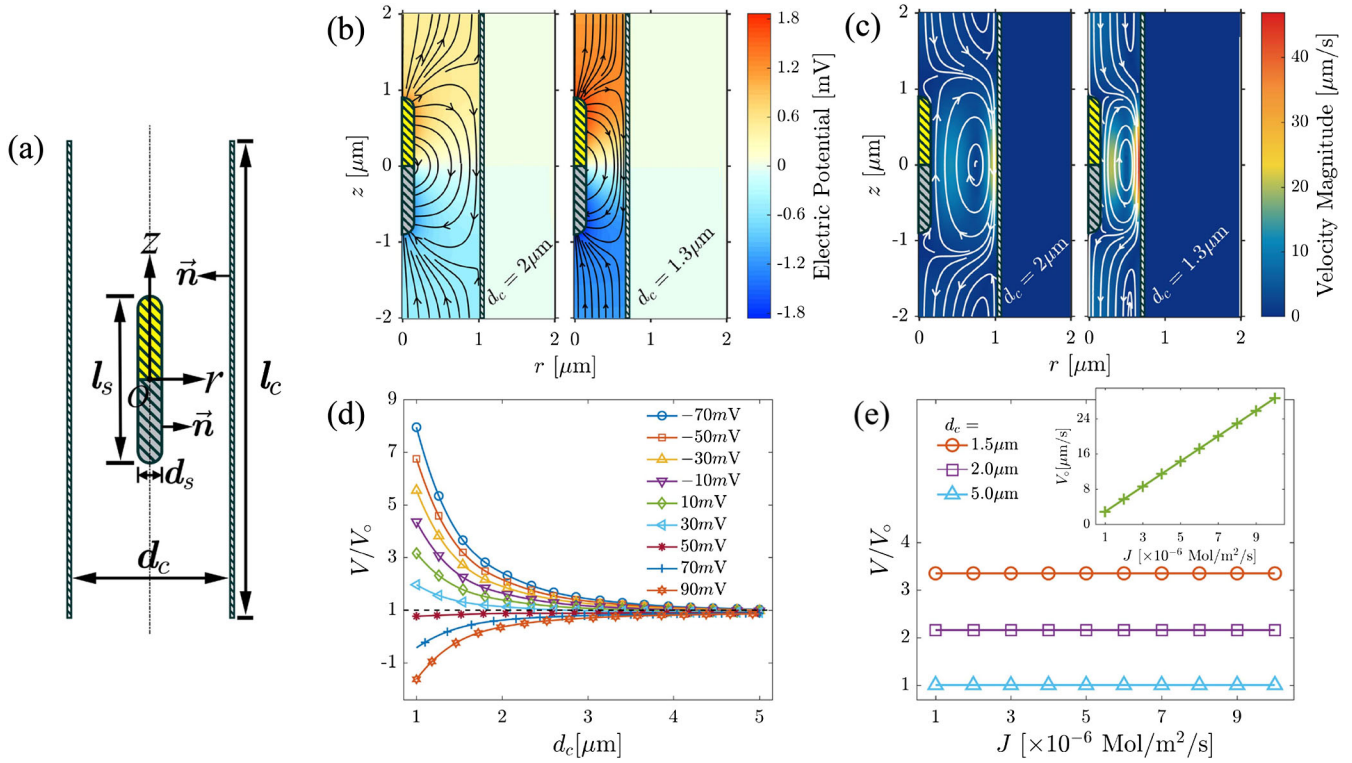

FIG. 2. (a) Schematic diagram of the model (not to scale). A cylindrical coordinate frame (r, z) is defined with the origin located at the center of the swimmer; the local normal direction on the swimmer and channel surfaces is denoted as $\vec{n}$. Dimensions of the swimmer and channel are defined. The anode and cathode of the swimmer is shown in yellow and gray, respectively. (b)–(c) Electric potential and fluid flow around a stalled swimmer ($V = 0$) in channels. Lines in (b) and (c) represent the electric field and stream lines, respectively. To produce results in Fig. 2(c), we set the swimmer zeta potential to zero ($\zeta_s = 0$) so that only electro-osmotic flow on the channel surface (not on the swimmer surface) is generated. (d)–(e) Normalized swimmer velocity versus the channel width d_c and the reaction flux J. The legend of (d) shows the channel zeta potential used for each data set. Default values (see text) are used for simulation parameters that are not specified in (b)–(e).

depends on the channel geometry but not on the driving strength.

To understand these findings and to investigate the phenomenon in an extended parameter regime, we turn to an electrokinetic numerical model, which was originally used by Velegol *et al.* to study spherical self-electrophoretic swimmers near a plane [39,58]. Our model assumes axial symmetry. As shown in Fig. 2(a), a rodlike microswimmer moves with a velocity $V\vec{e}_z$ along the center line of a circular channel. The swimmer and the channel have respective zeta potentials: ζ_s and ζ_c. The electric double layers are assumed to be infinitely thin [19–22,56,58–61] and charge neutrality decouples proton concentration from the model that consists of electrostatic and electrohydrodynamic parts. The electrostatic problem is defined by the Laplace equation ($\nabla^2\phi = 0$) for the electric potential ϕ and the boundary conditions on solid surfaces. On the swimmer [19,39,58,61], proton generation and absorption on the anode and cathode, respectively, lead to normal potential gradients: $-(\partial\phi/\partial n) = (Jk_BT/2eDn_\circ)$ and $-(\partial\phi/\partial n) = (-Jk_BT/2eDn_\circ)$, where J is the magnitude of the proton flux and other parameters (k_B, T, e, D, and $n_\circ$) are defined in the Supplemental Material [48]. No reaction occurs on the channel surface: $(\partial\phi/\partial n) = 0$. The electrohydrodynamic problem is governed by the Stokes flow: $\mu\nabla^2\vec{u} - \nabla p = 0$ and $\nabla\cdot\vec{u} = 0$, where μ is the fluid viscosity. Flow boundary conditions are determined by the solid motion and the slip electro-osmotic surface flow [20]; we have $\vec{u} = (\epsilon\zeta_c/\mu)(\overleftrightarrow{I} - \vec{n}\,\vec{n})\cdot\nabla\phi$ on the stationary channel and $\vec{u} = V\vec{e}_z + (\epsilon\zeta_s/\mu)(\overleftrightarrow{I} - \vec{n}\,\vec{n})\cdot\nabla\phi$ on the swimmer, where $\overleftrightarrow{I}$ is the unit tensor and ϵ is the fluid permittivity. Finally, the swimmer velocity V is determined by the force balance condition: $F_z = \vec{e}_z\cdot\oint_{\text{swimmer}}\overleftrightarrow{\sigma}\cdot d\vec{S} = 0$, where $\overleftrightarrow{\sigma}$ is the stress on the swimmer.

The model is solved by a finite-element package (COMSOL Multiphysics). Implementation details and calibration studies can be found in the Supplemental Material [48]. We use the following default parameters in simulations unless specified otherwise: $d_s = 0.3$ μm, $l_s = 1.8$ μm, $l_c = 16$ μm, $d_c = 2$ μm, $J = 7\times10^{-6}$ mol/m²/s, $\zeta_s = -50$ mV, and $\zeta_c = -50$ mV, where two swimmer parameters (J and ζ_s) and the channel zeta potential (ζ_c) are chosen according to measurements in Refs. [18,62] and [63,64], respectively.

The channel enters our model through the electrostatic and electrohydrodynamic boundary conditions. To visualize its effects, we plot the electric and flow fields around a stalled swimmer ($V = 0$). As shown in Fig. 2(b), the channel screens the electric field; narrower channel leads to a larger potential gradient and, therefore, stronger electro-osmotic flow on the swimmer surface to facilitate its motion in the $\vec{e}_z$ direction. The second effect comes from the negatively charged channel surface. As shown in Fig. 2(c), the electric field generates a downward electro-osmotic flow on the channel; this localized and confined flow creates an upward backflow near the swimmer due to fluid continuity. The backflow generates an upward force on the stalled swimmer, which is 0.16 and 0.64 pN for the case of $d_c = 2$ μm and $d_c = 1.3$ μm, respectively.

We next use the numerical model to reproduce two experimental findings in Fig. 1. For a negatively charged ($\zeta_c < 0$) channel, the model predicts that the swimmer velocity increases as the channel diameter decreases [Fig. 2(d)], which agrees with experiments. Quantitatively, in a linear channel with a cross section area of 2 μm^2, we have $V/V_\circ \approx 2$ from experiments (cf. Fig. 1) and $V/V_\circ = 2.8$ from simulations with the channel zeta potential $\zeta_c = -50$ mV [64]. Such an agreement is acceptable, considering the assumptions made in the model. Second, we change the proton flux J in simulations to explore the effect of the driving strength. As shown in Fig. 2(e), the swimmer velocities outside the channel $V_\circ$ increase linearly with the flux J but the normalized velocity $V/V_\circ$ is independent of the flux, which is in agreement with the experimental results in Figs. 1(e)–1(f). Independence on the driving strength suggests that catalytic reactions on the swimmer surface are reaction-limited and swimmer velocity is linearly related to the driving strength both in and outside the channel.

In addition, the numerical model allows us to explore the effect of the channel zeta potential ζ_c, which is difficult to change in experiments. Because the electro-osmotic flow is linearly related to ζ_c, as we reduce the negative charge on the channel, the facilitating backflow [Fig. 2(c)] becomes weaker and the swimmer velocity in the channel decreases, as shown in Fig. 2(d). When ζ_c becomes positive, the backflow reverses its direction and hinders the swimmer motion. At $\zeta_c = 50$ mV, the hindering backflow approximately cancels the facilitating electrostatic effect and $V/V_\circ$ is approximately 1. Further increasing ζ_c slows the swimmer down and eventually reverses its motion direction ($V/V_\circ < 0$).

To further explore the parameter space, we vary the swimmer length l_s in simulations. Outside the channel, swimmer velocity decreases with the swimmer length (inset of Fig. 3), which agrees with the analytic results in Refs. [21,22]. However, in channels, the swimmer length dependence changes qualitatively and the longer swimmers move faster (inset of Fig. 3), because the swimmer interacts with the boundary over its whole length to generate facilitating electrostatic and electrohydrodynamic effects (cf. Supplemental Material [48]). To verify this surprising simulation result, we fabricate AuRh swimmers of two different mean lengths (2.7 and 3.7 μm). Measurements of these AuRh swimmers are shown in Fig. 3 as solid symbols and confirm the model prediction; the longer AuRh swimmers speed up by 5 times in channels.

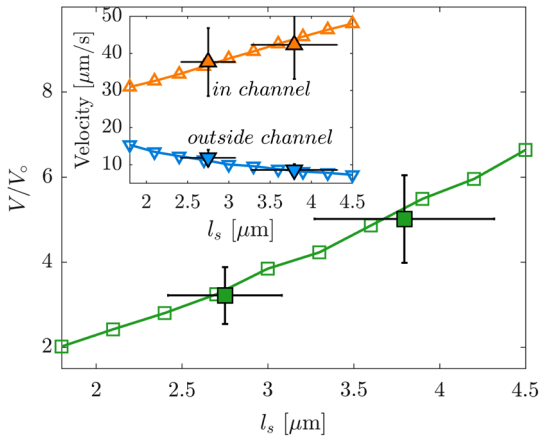

FIG. 3. Normalized swimmer velocity $V/V_\circ$ increases with the swimmer length. Swimmer velocities inside and outside channels are shown in the inset. Numerical and experimental data are shown by open and solid symbols, respectively. Experimental data are measured with AuRh swimmers in linear channels with $w = 1.2$ and $h = 2$ μm; Solutions with 15% H_2O_2 are used. Default values (see text) are used for simulation parameters except $J = 6 \times 10^{-6}$ mol/m^2/s and $d_c = 2.3$ μm.

Discussion.—In conventional electrophoretic experiments, an externally imposed electric field fills the system and drives electro-osmotic flow over the whole channel surface [59,60]. This is in clear contrast with the localized electric and flow fields around phoretic swimmers and leads to qualitatively different behaviors. For example, the velocity of externally driven particles decreases as the confinement (with surface charges of the same sign) becomes tighter [59,60] and more elongated particles move more slowly in confinement [60].

Previous studies have shown spatial confinement affects hydrodynamic swimmers through no-slip flow condition at boundaries [31–38]. For synthetic swimmers, new confinement effects appear because boundaries alters both scalar (concentration, temperature, or electric potential) and flow fields [39–47]. In a theoretical study of strong confinement, Popescu *et al.* [47] found that spherical boundary induces an accelerating phoretic and a decelerating hydrodynamic effect on a diffusiophoretic sphere. These two canceling effects result in a small increase of swimmer velocity. Chiang and Velegol [39] numerically studied an electrophoretic sphere near a flat surface and found that electro-osmotic surface flow slows down the swimmer if the

surface and swimmer are both negatively charged. This [39] and other investigations on swimmers near open boundaries [39–45] show confinement effects different from our reported speed enhancement, highlighting the critical role of confinement topology and its consequence on swimmer motility.

Essential ingredients of our model, such as diffusive driving field and slip surface flow, also appear in models for diffusiophoretic and thermophoretic swimmers [21,22]. Similar confinement effects may exist in some of these systems. For example, Brown *et al.* reported that a Pt/PS swimmer changes it speed when confined in a colloidal crystal [46]. However, intricate confining geometry, complex propulsion mechanisms [65,66], and lack of systematic data make it difficult to identify possible reasons for swimmer speed change in Ref. [46].

Last, synthetic swimmers were found to follow open boundaries and researchers suggested to use this property to steer swimmers [42,43]. Our work shows strongly confining channels can not only steer bimetallic swimmers but also modulate their velocities. This offers additional possibilities in controlling bimetallic swimmers. Therefore, tight spatial confinement may be a generally applicable control method for phoretic microswimmers.

We acknowledge financial support of the NSFC (No. 11422427, No. 11402069), the Program for Professor of Special Appointment at Shanghai Institutions of Higher Learning (No. SHDP201301), the Innovation Program of Shanghai Municipal Education Commission (No. 14ZZ030), and the government of Shenzhen (Grant No. KQCX20140521144102503). We thank Xiangjun Xing for useful discussions and Thomas Mallouk for his help with preparing the bimetallic microswimmers.

*To whom correspondence should be addressed.
hepeng_zhang@sjtu.edu.cn

[1] T. M. Squires and S. R. Quake, Rev. Mod. Phys. **77**, 977 (2005).
[2] P. Hanggi and F. Marchesoni, Rev. Mod. Phys. **81**, 387 (2009).
[3] E. Lauga and T. R. Powers, Rep. Prog. Phys. **72**, 096601 (2009).
[4] W. C. K. Poon, in *Physics of Complex Colloids, Proceedings of the International School of Physics "Enrico Fermi," Course 184*, edited by C. Bechinger, F. Sciortino, and P. Ziherl (IOS Press, Amsterdam, Netherlands, 2013), p. 317.
[5] I. S. Aranson, Phys. Usp. **56**, 79 (2013).
[6] J. Elgeti, R. G. Winkler, and G. Gompper, Rep. Prog. Phys. **78**, 056601 (2015).
[7] A. Zottl and H. Stark, J. Phys. Condens. Matter **28**, 253001 (2016).
[8] A. E. Patteson, A. Gopinath, and P. E. Arratia, Curr. Opin. Colloid Interface Sci. **21**, 86 (2016).
[9] W. Wang, W. Duan, S. Ahmed, T. E. Mallouk, and A. Sen, Nano Today **8**, 531 (2013).
[10] S. Sanchez, L. Soler, and J. Katuri, Angew. Chem., Int. Ed. **54**, 1414 (2015).
[11] H. R. Jiang, N. Yoshinaga, and M. Sano, Phys. Rev. Lett. **105**, 268302 (2010).
[12] J. R. Howse, R. A. L. Jones, A. J. Ryan, T. Gough, R. Vafabakhsh, and R. Golestanian, Phys. Rev. Lett. **99**, 048102 (2007).
[13] I. Buttinoni, J. Bialke, F. Kummel, H. Lowen, C. Bechinger, and T. Speck, Phys. Rev. Lett. **110**, 238301 (2013).
[14] J. Palacci, S. Sacanna, A. P. Steinberg, D. J. Pine, and P. M. Chaikin, Science **339**, 936 (2013).
[15] W. F. Paxton, K. C. Kistler, C. C. Olmeda, A. Sen, S. K. St Angelo, Y. Y. Cao, T. E. Mallouk, P. E. Lammert, and V. H. Crespi, J. Am. Chem. Soc. **126**, 13424 (2004).
[16] S. Fournier-Bidoz, A. C. Arsenault, I. Manners, and G. A. Ozin, Chem. Commun. **2005**, 441 (2005).
[17] Y. Wang, R. M. Hernandez, J. Bartlett, J. David, J. M. Bingham, T. R. Kline, A. Sen, and T. E. Mallouk, Langmuir **22**, 10451 (2006).
[18] W. Wang, T.-Y. Chiang, D. Velegol, and T. E. Mallouk, J. Am. Chem. Soc. **135**, 10557 (2013).
[19] A. Nourhani, P. E. Lammert, V. H. Crespi, and A. Borhan, Phys. Fluids **27**, 012001 (2015).
[20] J. L. Anderson, Annu. Rev. Fluid Mech. **21**, 61 (1989).
[21] R. Golestanian, T. B. Liverpool, and A. Ajdari, New J. Phys. **9**, 126 (2007).
[22] A. Nourhani and P. E. Lammert, Phys. Rev. Lett. **116**, 178302 (2016).
[23] J. Burdick, R. Laocharoensuk, P. M. Wheat, J. D. Posner, and J. Wang, J. Am. Chem. Soc. **130**, 8164 (2008).
[24] J. Wang, Lab Chip **12**, 1944 (2012).
[25] D. Kagan, P. Calvo-Marzal, S. Balasubramanian, S. Sattayasamitsathit, K. M. Manesh, G. U. Flechsig, and J. Wang, J. Am. Chem. Soc. **131**, 12082 (2009).
[26] J. Wu, S. Balasubramanian, D. Kagan, K. M. Manesh, S. Campuzano, and J. Wang, Nat. Commun. **1**, 36 (2010).
[27] L. Soler, V. Magdanz, V. M. Fomin, S. Sanchez, and O. G. Schmidt, ACS Nano **7**, 9611 (2013).
[28] B. Jurado-Sanchez, S. Sattayasamitsathit, W. Gao, L. Santos, Y. Fedorak, V. V. Singh, J. Orozco, M. Galarnyk, and J. Wang, Small **11**, 499 (2015).
[29] F. Ginot, I. Theurkauff, D. Levis, C. Ybert, L. Bocquet, L. Berthier, and C. Cottin-Bizonne, Phys. Rev. X **5**, 011004 (2015).
[30] P. Denissenko, V. Kantsler, D. J. Smith, and J. Kirkman-Brown, Proc. Natl. Acad. Sci. U.S.A. **109**, 8007 (2012).
[31] S. Jana, S. H. Um, and S. Jung, Phys. Fluids **24**, 041901 (2012).
[32] J. Mannik, R. Driessen, P. Galajda, J. E. Keymer, and C. Dekker, Proc. Natl. Acad. Sci. U.S.A. **106**, 14861 (2009).
[33] L. Zhu, E. Lauga, and L. Brandt, J. Fluid Mech. **726**, 285 (2013).
[34] A. Acemoglu and S. Yesilyurt, Biophys. J. **106**, 1537 (2014).
[35] H. Wu, M. Thiebaud, W. F. Hu, A. Farutin, S. Rafai, M. C. Lai, P. Peyla, and C. Misbah, Phys. Rev. E **92**, 050701 (2015).

[36] B. U. Felderhof, Phys. Fluids **22**, 113604 (2010).
[37] B. Liu, K. S. Breuer, and T. R. Powers, Phys. Fluids **26**, 011701 (2014).
[38] R. Ledesma-Aguilar and J. M. Yeomans, Phys. Rev. Lett. **111**, 138101 (2013).
[39] T. Y. Chiang and D. Velegol, Langmuir **30**, 2600 (2014).
[40] W. E. Uspal, M. N. Popescu, S. Dietrich, and M. Tasinkevych, Soft Matter **11**, 434 (2015).
[41] Y. Ibrahim and T. B. Liverpool, Europhys. Lett. **111**, 48008 (2015).
[42] S. Das, A. Garg, A. I. Campbell, J. Howse, A. Sen, D. Velegol, R. Golestanian, and S. J. Ebbens, Nat. Commun. **6**, 8999 (2015).
[43] J. Simmchen, J. Katuri, W. E. Uspal, M. N. Popescu, M. Tasinkevych, and S. Sanchez, Nat. Commun. **7**, 10598 (2016).
[44] A. Mozaffari, N. Sharifi-Mood, J. Koplik, and C. Maldarelli, Phys. Fluids **28**, 053107 (2016).
[45] D. Takagi, J. Palacci, A. B. Braunschweig, M. J. Shelley, and J. Zhang, Soft Matter **10**, 1784 (2014).
[46] A. T. Brown, I. D. Vladescu, A. Dawson, T. Vissers, J. Schwarz-Linek, J. S. Lintuvuori, and W. C. K. Poon, Soft Matter **12**, 131 (2016).
[47] M. N. Popescu, S. Dietrich, and G. Oshanin, J. Chem. Phys. **130**, 194702 (2009).
[48] See Supplemental Material at http://link.aps.org/supplemental/10.1103/PhysRevLett.117.198001 for fabrication procedures, studies of spiral channels, numerical implementation, supporting videos, and Refs. [49–52].
[49] M. Malinauskas, M. Farsari, A. Piskarskas, and S. Juodkazis, Phys. Rep. **533**, 1 (2013).
[50] J. L. Moran and J. D. Posner, J. Fluid Mech. **680**, 31 (2011).
[51] O. Schnitzer and E. Yariv, Phys. Fluids **27**, 031701 (2015).
[52] J. Happel and H. Brenner, *Low Reynolds Number Hydrodynamics* (Prentice Hall, Englewood Cliffs, 1965).
[53] J. L. Moran, P. M. Wheat, and J. D. Posner, Phys. Rev. E **81**, 065302 (2010).
[54] W. F. Paxton, P. T. Baker, T. R. Kline, Y. Wang, T. E. Mallouk, and A. Sen, J. Am. Chem. Soc. **128**, 14881 (2006).
[55] J. L. Moran and J. D. Posner, Phys. Fluids **26**, 042001 (2014).
[56] B. Sabass and U. Seifert, J. Chem. Phys. **136**, 214507 (2012).
[57] M. J. Esplandiu, A. A. Farniya, and D. Reguera, J. Chem. Phys. **144**, 124702 (2016).
[58] T. R. Kline, J. Iwata, P. E. Lammert, T. E. Mallouk, A. Sen, and D. Velegol, J. Phys. Chem. B **110**, 24513 (2006).
[59] H. J. Keh and J. L. Anderson, J. Fluid Mech. **153**, 417 (1985).
[60] C. Z. Ye, D. Sinton, D. Erickson, and D. Q. Li, Langmuir **18**, 9095 (2002).
[61] E. Yariv, Proc. R. Soc. A **467**, 1645 (2011).
[62] G. M. Dougherty, K. A. Rose, J. B. -H. Tok, S. S. Pannu, F. Y. S. Chuang, M. Y. Sha, G. Chakarova, and S. G. Penn, Electrophoresis **29**, 1131 (2008).
[63] S. Aura, T. Sikanen, T. Kotiaho, and S. Franssila, Sensors and Actuators B: Chemical **132**, 397 (2008).
[64] T. Sikanen, S. Aura, L. Heikkila, T. Kotiaho, S. Franssila, and R. Kostiainen, Anal. Chem. **82**, 3874 (2010).
[65] A. Brown and W. Poon, Soft Matter **10**, 4016 (2014).
[66] S. Ebbens, D. A. Gregory, G. Dunderdale, J. R. Howse, Y. Ibrahim, T. B. Liverpool, and R. Golestanian, Europhys. Lett. **106**, 58003 (2014).